DYNAMIC DRAINAGE AND IMBIBITION IMAGED USING FAST X-RAY MICROTOMOGRAPHY

M. Andrew, H. Menke, M. J. Blunt & B. Bijeljic
Imperial College London, Department of Earth Sciences & Engineering, London SW7 2AZ, UK

This paper was prepared for presentation at the International Symposium of the Society of Core Analysts held in St. John's, Newfoundland, 16-21 August, 2015

ABSTRACT

Recent developments in X-ray microtomography have allowed for multiple fluids to be imaged directly in the pore space of natural rock with temporal resolutions of tens of seconds, allowing for the direct observation of pore-scale displacements . This technique was used to image, with a spatial resolution of 3.64 μm and a temporal resolution of 45 seconds, the injection of supercritical CO_2 (drainage) and brine (imbibition) into a carbonate sample at conditions of pressure, temperature and salinity representative of subsurface flow (10 MPa, 50^{o}C, 1.5 M) using a novel technique for flow control at extremely low flow rates. Capillary pressure was measured from the images by finding the curvature of terminal menisci of both connected and disconnected CO_2 clusters, identified using local curvature anisotropy.

Snap-off in this system was examined by analysing a single snap-off event during drainage and imbibition. Capillary equilibrium concepts do not explain the low capillary pressures seen in the snapped off regions of the pore-space during drainage. The disconnected region created during drainage instead preserves the extremely low dynamic capillary pressures generated during a drainage event (Haines jump). Imbibition appeared isotropic with no clear macroscopic gradients in saturation developed. Snap-off in this system appears to be an equilibrium process, with no observable difference in interface curvature between the connected and disconnected non-wetting phase regions generated after snap-off.

INTRODUCTION

Recent developments in rapid synchrotron-based microtomography have, for the first time, allowed researchers to examine systems with a temporal resolution sufficient for the imaging of dynamic displacement processes, with pioneering papers by Berg *et al.*[1] and Armstrong *et al.* [2] examining Haines jumps and capillary desaturation respectively. At the same time recent developments have shown that, as microtomography is non-invasive, it is possible to conduct experiments at representative subsurface conditions, investigating capillary trapping [3, 4, 5, 6] and measuring contact angle [7, 8]. Synchrotron imaging at representative subsurface conditions has been used to examine multiple points of changing capillary pressure during drainage [9], however temporally resolved studies have still remained a challenge.

Multiphase flow is controlled by a complex set of variables, such as pore structure, interfacial tension and wettability. These are in turn a function of system conditions such as pressure, temperature, and salinity, e.g. Espinoza & Santamarina [10]. In such a complex system the experiments of flow processes at representative subsurface conditions becomes highly attractive. We present results from experiments examining drainage and imbibition conducted on the CO_2-brine-carbonate system at 10 MPa and 50^{o}C, conditions representative of subsurface flow in reservoirs and aquifers.

Drainage, or the injection of non-wetting phase (CO_2) into a porous medium saturated with wetting phase (brine), is extremely complicated in reservoir rocks. A qualitative understanding of the process at the pore-scale can be found using a network-based approximation of the pore-space, where the arbitrarily complicated pore-space is simplified into geometric and well-defined pores, connected by equally well-defined throats. Using this description drainage can be described using invasion percolation theory where the non-wetting phase (CO_2) displaces the wetting phase (brine) from each pore in a sequence of pore-scale events called Haines jumps [11]. These jumps represent the change between two states at capillary equilibrium, however as the jumps tend to proceed on the millisecond time-scale [12, 13], the dynamics of the transition between these two equilibrium states may display disequilibrium features [14]. Although these features (such as low dynamic capillary pressure) are transient, disappearing in connected regions of non-wetting phase as the system re-equilibrates after the transition (and so inaccessible to dynamic tomography with a temporal resolution of 45s), they may be preserved if regions of the pore-space filled with CO_2 are disconnected from the rest of the connected non-wetting phase prior to interface re-equilibration [15]. We present an example of such a phenomenon, showing that snap-off during drainage is due to a disequilibrium process.

In contrast, during imbibition (brine injection) regions of the pore-space full of wetting phase appear to swell uniformly over the length scale of the sample, with no clear fluid front developing. In this case snap-off occurs when the capillary pressure in a throat falls below the threshold snap-off capillary pressure of that throat, causing the throat to rapidly fill with brine, disconnecting a region of non-wetting phase from the rest of the (connected) non-wetting phase. We show that in this case there is no dis-equilibrium between the connected and disconnected non-wetting phase regions, at the point of snap-off, shown by the fact that there is no difference in their interface curvatures after snap-off is complete.

EXPERIMENTAL METHODS

The core assembly is shown in figure 1 and experimental apparatus shown in figure 2. The principal challenges when imaging the dynamic displacement of fluids at representative subsurface flow conditions are associated with system dead volume. The equipment used to control flow at high pressure includes large syringe pumps, connected to the core using long lengths of flexible tubing. Imaging the CO_2-brine system increases

these problems, as system dead volume is further increased by the incorporation of large batch reactors used to control fluid-fluid and fluid-solid reactions. This means that the dead volume of the system (defined as all the volume of fluid outside the rock core, estimated at around 1L) is many orders of magnitude greater than the internal pore-volume of the core (<0.5ml). Small changes in ambient temperature (or errors in the temperature control of heated elements of the system) cause changes in volume of the fluids in the system, potentially causing flow through the core. At high flow rates, such as those used in traditional core-flooding experiments, and in experiments imaging fluid distributions at the end of displacement processes, this is typically not an issue, as any induced flow by these changes in temperature is typically small compared to the flow rate applied across the core [4].

At the very low flow rates required for the examination of dynamic flow, however, flow induced by these changes in system dead-volume becomes important. In order to better constrain the flow boundary conditions for the core we propose a new micro-flow arrangement. A constant pressure drop is applied across a low permeability porous plate on the outlet face of the core (Figure 1). As this plate has a much lower permeability than the rock (with a rock to disk permeability ratio of around 1:200,000) essentially the entire of the applied pressure drop occurs across the plate. As the plate has a high capillary entry pressure, it remains saturated, resulting in a steady wetting phase (brine) flow through it. In this method a constant and extremely low flow rate boundary condition is applied directly at the outlet face of the core. In this way, changes in system volume are accommodated by changes in pump volume (pumps 1 and 3), rather than across the core. For this a hydrophilic modified semi-permeable disk (aluminium silicate, Weatherford Laboratories, Stavanger, Norway) of dimensions 4mm in diameter and 4mm in length and a permeability of 14×10^{-17} m^2 (14×10^{-6} D) was used. In this experiment flow rates of 1.75×10^{-15} m^3/s, equating to a capillary number of 1.10×10^{-11}**.**

Experiments were conducted on a single carbonate sample, Ketton Limestone, an Oolitic Grainstone from the Upper Lincolnshire Limestone Member (deposited 169-176 million years ago). Small cores around 4mm in diameter and 10-20mm in length were drilled from a large core plug around 38mm in diameter. The low permeability porous plate was mounted at the outlet face of the core and both were wrapped in aluminium to prevent diffusive CO_2 exchange across the confining sleeve. An X-ray transparent 4mm outer diameter polymeric tube was placed at the inlet face of the core so that the CO_2-brine interface could be easily monitored during pressurization prior to drainage. The core was then placed in a flouro-polymer elastomer (Viton) sleeve, which was attached to metal fittings connecting the core to the pore-fluid flow lines. A thermocouple was mounted near the base of the core outside the viton sleeve, which was then wrapped twice more with aluminium foil and placed within a high-temperature high-pressure Hassler type flow cell. The thermocouple was connected to a custom PID temperature controller, which heated the cell using an external Kapton insulated flexible heater. The position of the thermocouple is crucial for accurate temperature control, and by siting it in the

confining annulus by the base of the core it is possible to have a constant temperature xin the cell throughout the experiment.
The brine used was Potassium Iodide (KI) with a salinity of 1.5M. In order to prevent reaction between the carbonate rock and carbonic acid formed when $scCO_2$ is mixed with brine the three phases were mixed together prior to injection in a heated reactor. High-pressure syringe pumps were used to maintain system pressure and control the flow of fluids with an incremental displacement resolution of 25.4nL.

The experimental protocol is as follows:

- Raise the pressure and temperature in the reactor to that desired for the pore fluid during the experiment (50^{o}C and 10MPa).
- Load the core into the coreholder without the flowlines connected to the pumps, and establish a confining pressure of 1 MPa in the cell. This is to establish the same conditions of differential pressure (with the confining pressure 1 MPa above the pore pressure) as during the experiment.
- Centre the core in the field of view.
- Image the core along its entire length using a large number of projections (3600 per 180^o rotation). This creates a high quality unsaturated image from which the pore-space could be analysed in detail and to which saturated images could be compared.
- Bring the temperature of the coreholder up to the desired reservoir temperature.
- Bring the core up to reservoir pressures.
- At reservoir conditions there may be some constant offset between the readings in pumps 1 and 3, even if they were correctly calibrated at ambient conditions. In order to find this difference stop pump 3 while running pump 1 in constant pressure mode.
- Close valves 6, 7 and 8 then open valve 9. The difference between the pressure readings in pumps 1 and 3 will then be the pressure offset between the two pumps.
- Close valve 9 and open valves 6, 7 and 8. Reduce the pressure in pump 3, considering the transducer offset between pump 1 and 3, until there is a pressure drop of 5 kPa across the porous plate. This begins drainage.
- Begin taking scans. Exposure time and the number of projections per tomographic scan will depend specifically on the detector and synchrotron light source used. The results presented in this study were acquired using 800 projections with an exposure of 0.04s. from each image.
- The qualitative progress of the drainage process can be monitored without stopping the tomographic sequence by monitoring changes in the first radiograph.
- After drainage is complete, increase the pressure in pump 3 until it reaches 5 kPa pressure drop across the porous plate, in the opposite direction to that applied during drainage.
- Begin taking scans. Exposure time and the number of projections per tomographic scan will depend specifically on the detector and synchrotron light source use.

IMAGE ACQUISITION AND PROCESSING

Imaging was performed at Diamond Imaging Beamline I13 (Diamond Light Source, UK). Imaging was conducted under pink-beam conditions, with each scan taking around 45 seconds to acquire, with 32 seconds projections and around 13 seconds returning to the initial state and preparing for the next scan. To reduce the impact of beam heating on fluid distributions the pink-beam was then filtered by 2 mm of in-line graphite, 2 mm of in-line aluminium and 10 μm of in-line gold.

All image processing was conducted using Avizo Fire 8.0 and imageJ programs. Each image in the time-series was reconstructed using a filtered back projection algorithm[16], binned then cropped such that each image consisted of around 1100×1100×1100 voxels with a voxel size of 3.64 μm. The images were filtered using a non-local means denoising filter and registered to the first image in the dynamic sequence. The difference between each image and the first in the sequence (prior to non-wetting phase invading the pore-space during drainage) was computed for both drainage and imbibition, giving a high contrast map of non-wetting phase distributions. The time sequence of these maps of the non-wetting phase was then rendered in 3D to identify individual events of interest. Once these events had been identified subvolumes were extracted from the 4D data temporally located around each event. These subvolumes were then segmented using a seeded watershed algorithm [17]. Surfaces were generated across the non-wetting phase using a smoothed marching cubes algorithm [18], and interface curvature were calculated by approximating the surface locally as a quadratic form [15]. Terminal menisci from the wetting-non-wetting phase interface were identified using the anisotropy of the curvature vector (only taking measurements where the smallest principal radius of curvature of the interface was very close in magnitude to the largest principal radius of curvature). The radii of curvature of these regions of the wetting-non-wetting phase interface were maximised relative to the voxel size, making the estimation of mean curvature more reliable and were furthest away from the three phase contact line, minimising the impact of smoothing on resulting curvature distributions. Details about this technique will be included in an upcoming paper.

DRAINAGE

During drainage non-wetting phase invasion does not occur uniformly, but instead as a discrete set of events where regions of the pore-space which were previously occupied by wetting phase (brine) become occupied by non-wetting phase (CO_2) (Haines jumps [19]). The progress of these events is not resolved with the temporal resolution provided by synchrotron based dynamic tomography. Micromodels have been used to show that pores drain on the millisecond timescale, and that the time taken for the jump to occur is independent of the macroscopic capillary number [12, 13]. This behavior can be understood by describing these events and changes between two states at capillary equilibrium; before and after each of the non-wetting phase jumps. Dynamic tomography therefore allows us to see the sequence of these jumps during drainage, and by looking in detail at the fluid distributions before and after each of the jumps, we can examine and test some of the assumptions in descriptions of multi-phase flow. Specifically it allows us to examine the relative processes by which regions of non-wetting phase can become

isolated from the rest of the pore-space occupied by connected non-wetting phase in the process of snap-off. This is particularly interesting as the disconnected non-wetting phase region preserves the conditions present at the point of snap-off, even as flow continues around it.

Snap-off occurs during drainage by the following mechanism. As the wetting-non-wetting interface emerges from a pore throat during a drainage event, the curvature across that interface will decrease. This causes curvature disequilibrium between the leading region and other regions of the wetting-non-wetting phase interface. As the interface attempts to re-equilibrate, the curvature in the pore-throat connecting the leading portion on the non-wetting phase from the rest of the connected non-wetting phase starts to decrease. If the curvature in this throat decreases below the threshold snap-off capillary pressure for that throat, the leading portion of non-wetting phase will snap-off, disconnecting it from the rest of the connected CO_2.

This process can be seen in the experiments examined in this study in two successive tomographic scans in the 4D dataset, separated by 45 seconds (figure 3, A-B). Surface curvature is measured, using curvature anisotropy (the relative magnitude of the larger and smaller principal curvature vectors), for both the connected and disconnected CO_2 phase before and after the jump (figure 3C).

The interface curvatures measured on the disconnected ganglion are much lower than those of the connected CO_2 region either before or after the invasion – snap-off sequence has occurred. We propose that this is due to significant dynamic capillary pressure gradients generated in the leading region of the non-wetting phase during the drainage event, out of capillary equilibrium. These cause the low capillary pressures required for throat snap-off, which are then preserved in the disconnected ganglion. The capillary pressure of the ganglion is defined by the threshold snap-off capillary pressure of the disconnecting throat, defined by the local pore geometry, consistent with the findings of Andrew *et al.* [6], where the capillary pressures of a population of disconnected ganglia were observed to be controlled by local pore geometry (and so threshold snap-off capillary pressures). After the invasion/snap-off event has completed the rest of the connected non-wetting phase interface will re-equilibrate to some new stable interface curvature, however the disconnected region will not, thereby retaining and preserving the low dynamic curvatures generated during the invasion event on the time scale resolvable with synchrotron based microtomography.

IMBIBITION

During imbibition the wetting phase invades the pore-space in a uniform fashion, with no clear front developing over the length scale observable in the experiment. No macroscopic gradients in saturation (“front”) develop on the length-scale of the image as the connected wetting-non-wetting interface remains at capillary equilibrium (displaying no gradients in the interface curvature of the connected non-wetting-wetting phase interface). As capillary pressure decreases, corresponding to an increase in wetting phase

saturation, wetting phase regions appear to swell uniformly throughout the imaged volume.
If we look at snap-off in this system (during imbibition) the connected non-wetting phase curvature is not distinctly different before or after the snap-off event, and the disconnected non-wetting phase region curvature is not distinctly different to the connected non-wetting phase region either before or after the event (figure 4). These results can be understood by thinking of imbibition (and resulting snap-off) as an equilibrium process. As wetting layers swell during wetting phase invasion, capillary pressure slowly decreases across the entire wetting-non-wetting phase interface. When it gets below the threshold snap-off capillary pressure for a particular throat, that throat snaps off rapidly, but because prior to snap-off the entire wetting-non-wetting interface was at equilibrium, there is no gradient in capillary pressure between the connected and disconnected non-wetting phase regions. The connected non-wetting phase will then continue to be displaced out of the system by the invading wetting phase, reducing connected surface capillary pressure. The disconnected ganglion, however, will retain the capillary pressure present at snap-off.

This is in contrast to snap-off occurring during drainage, where dynamic forces generated by a Haines jump decrease curvature in a throat to below its threshold snap-off curvature. Because these changes in capillary pressure are due to dynamic forces (occurring on the millisecond time-scale), they are not represented in the curvature of the connected phase in the next image in the time sequence (with an image time resolution of around 45 seconds). As the capillary pressure of the disconnected phase is primarily controlled by the threshold snap-off capillary pressure, as defined by the local pore geometry, dynamic curvatures are preserved in the disconnected ganglion, creating a difference in interface curvature between connected and disconnected non-wetting phase regions.

CONCLUSIONS

We have used synchrotron based dynamic tomography to image the drainage (non-wetting phase invasion) and imbibition (wetting phase invasion) process in a carbonate sample at representative subsurface conditions with a time resolution of around 45 seconds. Snap-off has been observed in both processes, disconnecting non-wetting phase regions. Curvature distributions show a difference in interface curvature between the disconnected and connected non-wetting phase region after snap-off, whereas during imbibition there is no clear difference between the interface curvature distributions. We propose that this difference in interface curvature is due to a difference in the physics causing the snap-off in each system.

Snap-off in the drainage process is due to dynamic forces, arising due to low interface curvatures generated as a non-wetting phase (CO_2) region invades a region of the pore-space occupied by wetting phase (brine) in a Haines jump. This reduces interface curvatures in the invaded pore throat to below its threshold snap-off capillary pressure. Snap-off during imbibition, however, is due to the equilibrium swelling of wetting phase regions during brine invasion, until the threshold snap-off capillary pressure of a throat is

reached. At this point the throat rapidly fills with wetting phase, however prior to snap-off the interface was at equilibrium, meaning that the resulting connected and disconnected non-wetting phase regions have no difference in interface curvature.

Future work could focus on examining the relative statistical importance of snap-off processes during drainage, or the correlation of modelled snap-off capillary pressures to experimentally observed interface curvatures. Another interesting area for future research is how the results of these experiments at extremely low flow rates correspond to more rapid displacements seen in realistic subsurface conditions, and how the interaction between viscous pressure gradients, causing flow, and capillary forces can cause changes in pore-scale displacement processes on the individual pore and ganglion scales.

ACKNOWLEDGEMENTS

We thank Diamond Light Source for access to beamline I13 and especially the assistance of Dr. Christoph Rau and Dr. Joan Vila-Comamala who contributed to the results presented here. We acknowledge funding from the Imperial College Consortium on Pore-Scale modelling. We also gratefully acknowledge funding from the Qatar Carbonates and Carbon Storage Research Centre (QCCSRC), provided jointly by Qatar Petroleum, Shell, and Qatar Science & Technology Park.

REFERENCES

1. Berg, S. *et al.* Real-time 3D imaging of Haines jumps in porous media flow. *Proc. Natl. Acad. Sci. U. S. A.* **110,** 3755–9 (2013).
2. Armstrong, R. T., Georgiadis, A., Ott, H., Klemin, D. & Berg, S. Critical capillary number: Desaturation studied with fast X-ray computed microtomography. *Geophys. Res. Lett.* **41,** 55–60 (2014).
3. Andrew, M., Bijeljic, B. & Blunt, M. J. Pore-scale imaging of geological carbon dioxide storage under in situ conditions. *Geophys. Res. Lett.* **40,** 3915–3918 (2013).
4. Andrew, M., Bijeljic, B. & Blunt, M. J. Pore-scale imaging of trapped supercritical carbon dioxide in sandstones and carbonates. *Int. J. Greenh. Gas Control* **22,** 1–14 (2014).
5. Chaudhary, K. *et al.* Pore-scale trapping of supercritical CO2 and the role of grain wettability and shape. *Geophys. Res. Lett.* **40,** 3878–3882 (2013).
6. Andrew, M., Bijeljic, B. & Blunt, M. J. Pore-by-pore capillary pressure measurements using X-ray microtomography at reservoir conditions: Curvature, snap-off, and remobilization of residual CO2. *Water Resour. Res.* **50,** 8760–8774 (2014).
7. Aghaei, A. & Piri, M. Direct pore-to-core up-scaling of displacement processes: Dynamic pore network modeling and experimentation. *J. Hydrol.* **522,** 488–509 (2015).
8. Andrew, M., Bijeljic, B. & Blunt, M. J. Pore-scale contact angle measurements at reservoir conditions using X-ray microtomography. *Adv. Water Resour.* **68,** 24–31 (2014).

9. Herring, A. L., Andersson, L., Newell, D. L., Carey, J. W. & Wildenschild, D. Pore-scale observations of supercritical CO2 drainage in Bentheimer sandstone by synchrotron x-ray imaging. *Int. J. Greenh. Gas Control* **25,** 93–101 (2014).
10. Espinoza, D. N. & Santamarina, J. C. Water-CO2-mineral systems: Interfacial tension, contact angle, and diffusionImplications to CO2 geological storage. *Water Resour. Res.* **46,** 1–10 (2010).
11. Wilkinson, D. & Willemsen, J. F. Invasion percolation: a new form of percolation theory. *J. Phys. A. Math. Gen.* **16,** 3365–3376 (1999).
12. Mohanty, K. K., Davis, H. T. & Scriven, L. E. Physics of Oil Entrapment in Water-Wet Rock. *SPE Reservoir Engineering* **2,** (1987).
13. Armstrong, R. T. & Berg, S. Interfacial velocities and capillary pressure gradients during Haines jumps. *Phys. Rev. E - Stat. Nonlinear, Soft Matter Phys.* **88,** 1–9 (2013).
14. Moebius, F. & Or, D. Pore scale dynamics underlying the motion of drainage fronts in porous media. *Water Resour. Res.* **50,** 8441–8457 (2014).
15. Armstrong, R. T., Porter, M. L. & Wildenschild, D. Linking pore-scale interfacial curvature to column-scale capillary pressure. *Adv. Water Resour.* **46,** 55–62 (2012).
16. Titarenko, V., Titarenko, S., Withers, P. J., De Carlo, F. & Xiao, X. Improved tomographic reconstructions using adaptive time-dependent intensity normalization. *J. Synchrotron Radiat.* **17,** 689–699 (2010).
17. Jones, A. C. *et al.* Assessment of bone ingrowth into porous biomaterials using MICRO-CT. *Biomaterials* **28,** 2491–2504 (2007).
18. Hege, H., Seebass, M., Stalling, D. & Zockler, M. A Generalized Marching Cubes Algorithm Based On Non-Binary Classifications. *ZIB Prepr.* **sc-97-05,** (1997).
19. Haines, W. B. Studies in the physical properties of soil. V. The hysteresis effect in capillary properties, and the modes of moisture distribution associated therewith. *The Journal of Agricultural Science* **20,** 97 (1930).

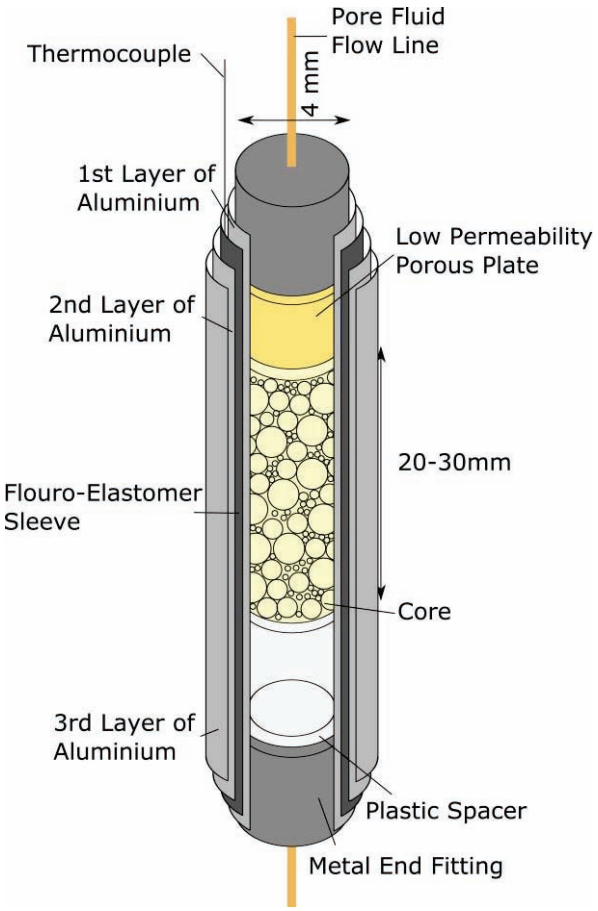

Figure 1: Core Assembly, showing the relative positioning of the low permeability porous plate, the core and the plastic space (allowing for the wetting-non-wetting interface to be seen prior to invasion in the core.

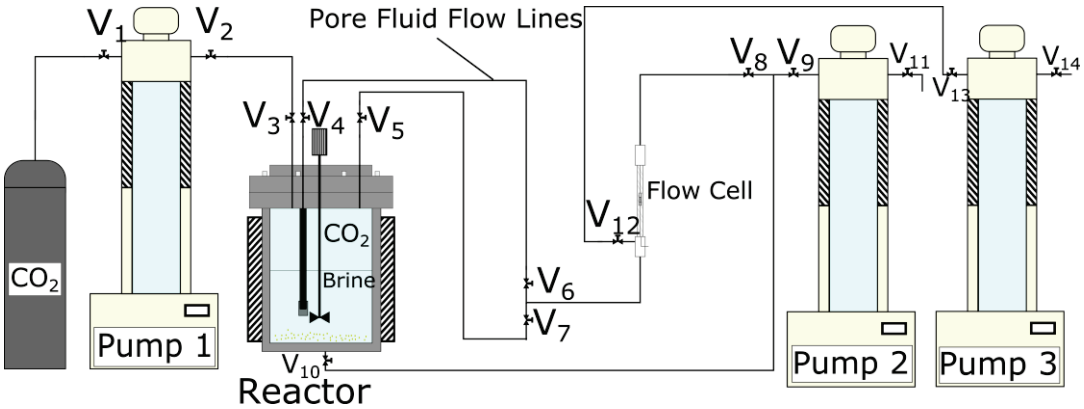

Figure 2: Experimental flow apparatus, showing how high-pressure syringe pumps were connected to the flow cell.

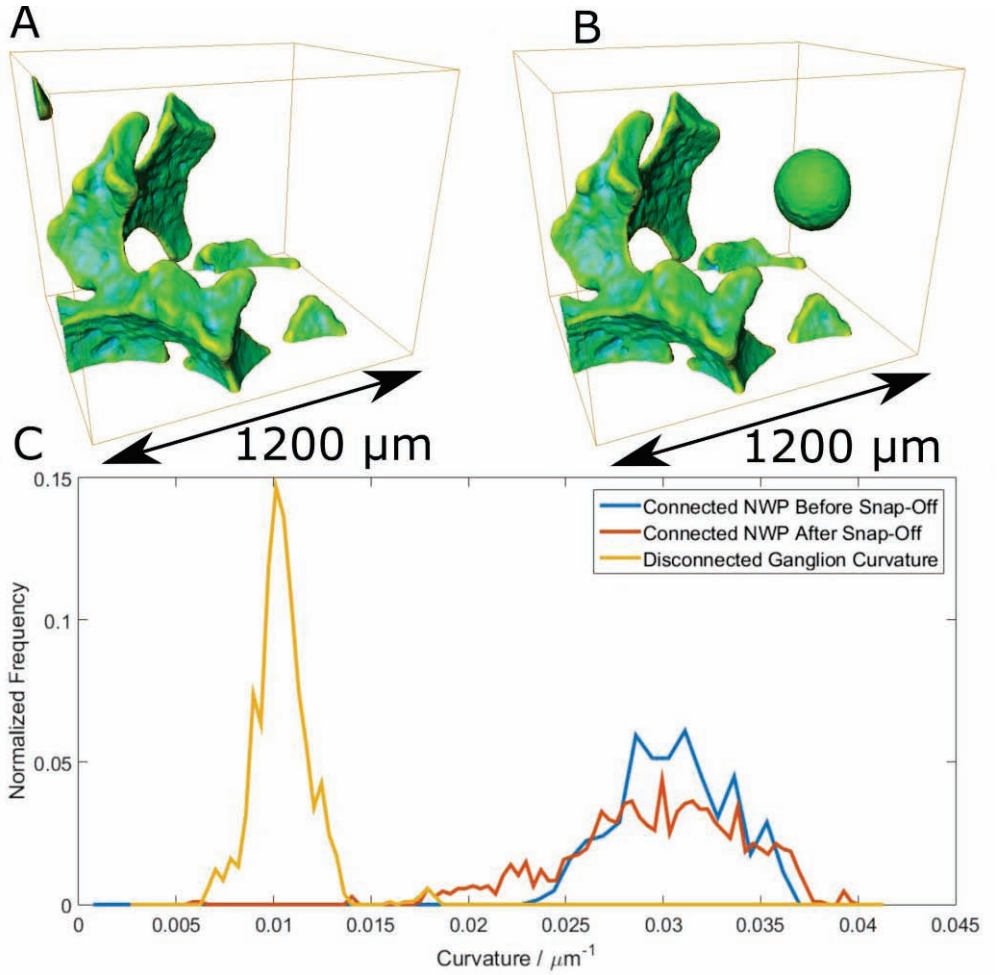

Figure 3: A-B: Connected and disconnected non-wetting phase (CO_2) after invasion & snap-off during drainage, taken from two subsequent tomographies. In this rendering the wetting phase (brine) and the rock grains are see-through. The surfaces are coloured according to the magnitude of the mean interface curvature. C: The distribution of curvatures, as measured on terminal menisci identified using curvature anisotropy. The disconnected non-wetting phase region formed by snap-off has a lower interface curvature than the connected non-wetting phase region either before or after the snap-off event.

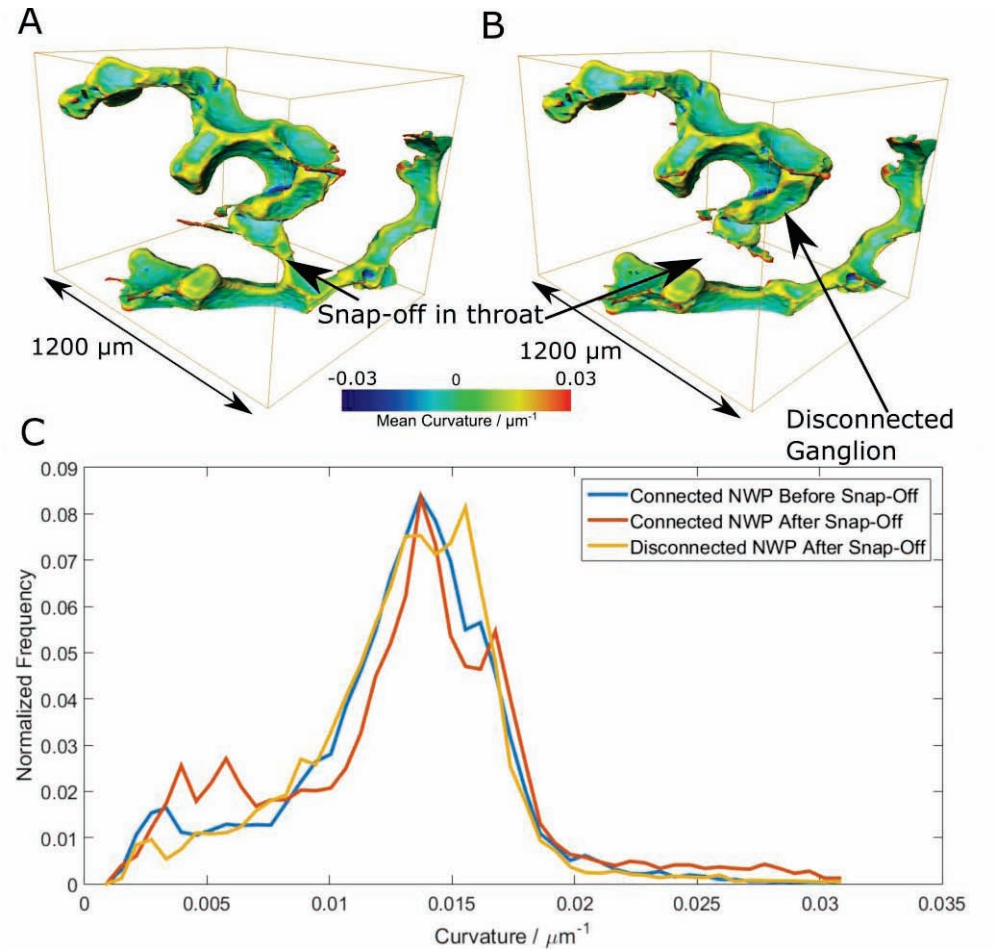

Figure 4: A-B: Connected and disconnected non-wetting phase (CO_2) after invasion & snap-off during imbibition, taken from two subsequent tomographies. In this rendering the wetting phase (brine) and the rock grains are transparent. The surfaces are coloured according to the magnitude of the mean interface curvature. C: The distribution of curvatures, as measured on terminal menisci from the wetting-non-wetting fluid-fluid interface, identified using curvature anisotropy. The disconnected non-wetting phase region formed by snap-off has an indistinguishable interface curvature to the connected non-wetting phase region either before or after the snap-off event.